THE JOURNAL OF PHYSICAL CHEMISTRY B

Article

Cite This: J. Phys. Chem. B 2019, 123, 974−982

pubs.acs.org/JPCB

# Rheological Tuning of Entangled Polymer Networks by Transient Cross-links

Xue-Zheng Cao and M. Gregory Forest*

Department of Mathematics and Applied Physical Sciences, University of North Carolina at Chapel Hill, Chapel Hill, North Carolina 27599, United States

**ABSTRACT:** The remarkable functionalities of transiently cross-linked, biopolymer networks are increasingly becoming translated into synthetic materials for biomedical and materials science applications. Various computational and theoretical models, representing different transient cross-linking mechanisms, have been proposed to mimic biological and synthetic polymer networks, and to interpret experimental measurements of rheological, transport, and self-repair properties. Herein, we employ molecular dynamics simulations of a baseline entangled polymer melt coupled with parametrized affinities for binding and unbinding of transient cross-links (CLs). From these assumptions alone, we determine the emergent CL mean density and fluctuations, and the induced rheology, across the 2-parameter space of binding and unbinding affinities for a moderately long chain, entangled the polymer melt. For sufficiently weak (short-lived) CLs, nonmonotonicity emerges with respect to the affinity to form CLs: the stress relaxation, viscous, and elastic moduli all shift above the baseline if CLs form rapidly, reverse below the baseline as CLs form slowly, and reverse again, recovering the baseline as CLs form very slowly. For sufficiently strong (long-lived) CLs and sufficiently fast CL formation, a dramatic rise emerges in the viscous and elastic moduli at all frequencies, more prominently in the elastic moduli at medium to high frequencies, inducing a sol−gel transition. These results are placed in context with the experimental and theoretical literature on transient polymer networks.

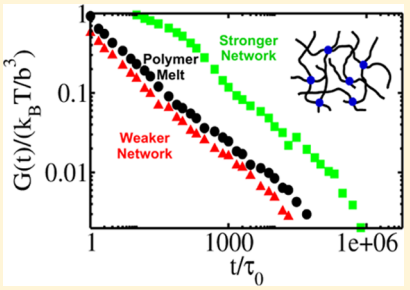




## INTRODUCTION

Transient polymer networks are ubiquitous in biology. Chromosomes in eukaryote cell nuclei are transiently cross-linked by structural maintenance of chromosome proteins.[1−4] Antibodies in mucosal layers that coat all internal mammalian organs transiently cross-link (CL) pathogens (viruses, bacteria) and foreign particulates to the mucin polymer mesh, thereby immobilizing the invasive species so that they can be cleared.[5−15] Mucus is itself a transiently cross-linked network of mucin polymers by scores of small molecule proteins.[9,16−22] Other transiently cross-linked biological polymer networks include associative polymer actin gels,[23,24] extracellular matrices,[25] and cytoplasmic molecular complexes.[26,27] Transient gels are also explored in materials engineering because of their reversible and self-healing properties[28−32] with diverse biomedical[33,34] and materials science[35−38] applications. For example, employing rationally engineered polymer nanoparticle interactions that control transient CLs, the Langer group has introduced a new paradigm for the fabrication of self-assembled and biocompatible hydrogels that are utilized for drug delivery.[39−43] There is a surge of interest in ionic liquids (ion hopping) and transient associative polymers, cf.,[44,45] recently surveyed in ref 46.

Compared to polymer networks cross-linked by permanent, covalent bonds, transient networks consist of many types of reversible binding interactions, for example, hydrogen bonds, metal−ligand coordination, ionic and electrostatic interactions, and hydrophobic associations. Although, an exploratory study of the effects of cross-linking kinetics on the rheological properties of entangled polymer networks is experimentally challenging, many labs cited above and elsewhere are doing so. Various theoretical models and mechanisms have been developed and applied to understand and predict macroscopic rheological properties and microscopic behavior across diverse lengthscales and timescales. From the sticky reptation model for associative polymers, with a predetermined number of stickers (i.e. density of active CLs) attached to each polymer chain at fixed positions along the chains, Rubinstein et al. reveal that the dynamical properties of reversible networks are governed primarily by the network strand size and by the effective lifetime of reversible junctions.[37,47−49] Using the percolation theory, Colby and collaborators quantitatively analyzed the linear viscoelastic response of lightly sulfonated, short-chain polystyrene and give insights into its reversible gelation properties.[44,46] In recent studies of focusing on Rouse chains undergoing head-to-head association and dissociation, Watanabe et al. confirmed that there are dynamic differences between dielectric and viscoelastic relaxation of Rouse chains.[50,51]

Our modeling approach is inspired by collaborations with experimental colleagues on various natural biopolymer networks including mucus[52,53] and chromosomal DNA.[1,2] Hult et al. extended the stochastic Rouse-like polymer bead-spring model of chromosomal DNA to incorporate transient binding

Received: September 25, 2018
Revised: January 8, 2019
Published: January 8, 2019




DOI: 10.1021/acs.jpcb.8b09357
J. Phys. Chem. B 2019, 123, 974−982

in the nucleolus on chromosome XII in living yeast.[1,2,54] The model results were compared with experimental data on live yeast, with best agreement for weak, short-lived binding kinetics. Similar to these models for chromosomes, we employ molecular dynamics (MD) simulations, leveraging the LAMMPS open-source software package (https://lammps.sandia.gov/), to explore how binding/unbinding kinetics of transient CLs self-select the mean density and fluctuations of active polymer domains, and thereby tune the rheological properties of a canonical baseline system: an entangled, relatively long chain polymer melt. Our model is distinct from previous studies in that we parametrize the affinity timescales for binding and unbinding among all "active" polymer domains and the mean density, fluctuations, and heterogeneous distribution of CLs across the network are emergent properties. The structure and rheology of the transient network are the consequences of these stochastic CL properties. This modeling framework is adaptable to other natural and synthetic polymer networks where the transient CLs have different affinities, from vanishingly weak to permanent, to the full spectrum of polymer domains.

## COMPUTATIONAL DETAILS

Using the open-source software LAMMPS, polymers are modeled as coarse-grained bead-spring chains without explicit twist or bending potential, that is, bonds are freely rotating and freely joined within the limits set by excluded-volume interactions with nearby beads. The beads with diameter $b$ represent spherical Kuhn monomers which interact via a shifted Lennard-Jones (LJ) potential

$$U_{\mathrm{LJ}}(r) = 4\epsilon_0\left[\left(\frac{b}{r}\right)^{12} - \left(\frac{b}{r}\right)^{6} - \left(\frac{b}{r_c}\right)^{12} + \left(\frac{b}{r_c}\right)^{6}\right] \quad (1)$$

where $r_c$ is the cut-off distance of the interaction, fixed at $r_c = 2.5b$ for all simulations. A finitely extensible nonlinear elastic (FENE) potential was used to define the connectivity (including covalent nearest-neighbor bonds and transient non nearest-neighbor CLs) between monomers (beads)

$$U_{\mathrm{FENE}}(r) = -0.5\kappa {R_0}^2 \ln\left[1 - \left(\frac{r}{R_0}\right)^2\right] + 4\epsilon_0\left[\left(\frac{d}{r}\right)^{12} - \left(\frac{d}{r}\right)^{6}\right] + \epsilon_0, \qquad r < R_0 \quad (2)$$

where $\kappa = 30\epsilon_0/b^2$ is the spring constant, $R_0 = 1.5b$ stands for the maximum extension of the bond, and $d = 1.2b$ for the covalent bonds and $d = b$ for the transient bonds.[55,56] The equation of motion of any bead in the implicit solvent (neglecting any hydrodynamic interaction) is given by the Langevin equation

$$m\frac{\mathrm{d}^2\mathbf{r}_i}{\mathrm{d}t^2} = -\nabla_i U - \zeta\frac{\mathrm{d}\mathbf{r}_i}{\mathrm{d}t} + \mathbf{W}_i(t) \quad (3)$$

where $m = m_0$ (with $m_0$ being the mass unit) is the monomer mass, $\mathbf{r}_i$ is the position of the $i$th bead, $\zeta = (\epsilon_0/m_0b^2)^{1/2}$ is the friction coefficient, and $U$ is the total conservative potential including FENE and LJ potentials acting on the $i$th bead. The quantity $\mathbf{W}_i(t)$ is a stochastic white noise force without drift and second moment proportional to the temperature and the friction coefficient $\zeta$. We include viscous drag on each bead but suppress hydrodynamic interactions between beads and chains (the free draining approximation).[57]

In the simulations of transiently cross-linked polymers, every polymer bead is capable of participating in a transient bond. Transient bond formation: a search for new transient CLs is performed every $\tau_B$, a chosen waiting time for encounters that is a proxy for the concentration of cross-linkers and their accessibility to binding sites on the chains. At every $\tau_B$, if the separation $r_{ij}$ between any two free beads $i$ and $j$ is smaller than a predefined critical distance $r_B = 1.0\sigma_0$ (fixed throughout this study), there is a probability $P_B$ of generating a transient bond between beads $i$ and $j$. This probability is a proxy for the strength of the affinity for a bond to form between the bead pair. Transient bond formation is thereby controlled by two tuning parameters, $\tau_B$ and $P_B$. Note that the beads are restricted divalent transient bonds for this study. Transient bond breakage: every bond that forms is maintained for a minimum waiting time, $\tau_U$, at which time the bond breaks with probability $P_U$, and every waiting time increment thereafter.

In the MD simulations, the stress relaxation modulus function $G(t)$ is quantitatively computed using a standard protocol relating $G(t)$ to the stress autocorrelation function SACF($t$) of off-diagonal elements of the system stress tensor based on the Green−Kubo relation:[58−60] $G(t) = \frac{V}{K_BT}\mathrm{SACF}(t)$, where $V$ is the system volume and the system temperature is fixed at $K_BT = \epsilon_0$ with $\epsilon_0$ being the energy unit in the MD simulations. The stress autocorrelation function (SACF) was computed from the formula

$$\mathrm{SACF}(t) = \frac{1}{3}[\langle\sigma_{xy}(t)\sigma_{xy}(0)\rangle + \langle\sigma_{yz}(t)\sigma_{yz}(0)\rangle + \langle\sigma_{xz}(t)\sigma_{xz}(0)\rangle] \quad (4)$$

where $\sigma_{xy}$, $\sigma_{yz}$, and $\sigma_{xz}$ are the off-diagonal elements of the stress tensor. The boundary conditions in all three directions are periodic. The simulations are carried out using the LAMMPS MD package at a constant temperature of $T = 1\epsilon_0/K_B$ and a fixed cubic box size of $l_{box}$, which is always chosen to be much larger than the radius of gyration of single chains, that is, $l_{box} \gg r_g$.

## RESULTS

**Baseline System: An Entangled, Homogeneous Polymer Melt (HPM).** The baseline system consists of identical, Rouse-like bead-spring chains, at entanglement concentrations. These specifications constitute a homogeneous polymer melt, denoted as HPM. (In future studies, we will consider molecular weight distributions of the polymers and mixtures of different polymers, e.g., the mucins MUC5AB and MUC5C in pulmonary mucus.) In highly entangled HPMs, the polymer chain length $L_c$ is significantly longer than the average contour length of polymer strands between entanglements (denoted as entanglement length $L_e$), that is, $L_c \gg L_e$. The stress relaxation modulus of highly entangled melts of ideal homogeneous polymer chains includes two regimes: the Rouse relaxation regime with $G_{\mathrm{HPM}}(t) = C_m \times k_BT\left(\frac{t}{\tau_m}\right)^{-0.5}$, when $t \ll \tau_e$, and the reptation regime because of entanglements with $G_{\mathrm{HPM}}(t) = G_e\exp\left(-\frac{t}{\tau_{ter}}\right)$, when $t \gg \tau_e$, where $C_m$, $\tau_m$, $\tau_e$, $\tau_{ter}$, and $G_e$ are the number density of monomers, the monomer relaxation time, the cross-over time between Rouse and



DOI: 10.1021/acs.jpcb.8b09357
J. Phys. Chem. B 2019, 123, 974−982

reptation relaxation, the terminal relaxation time of single chains, and the plateau modulus, respectively.[61] As shown in Figure 1, the stress relaxation modulus $G_{HPM}(t)$ for the

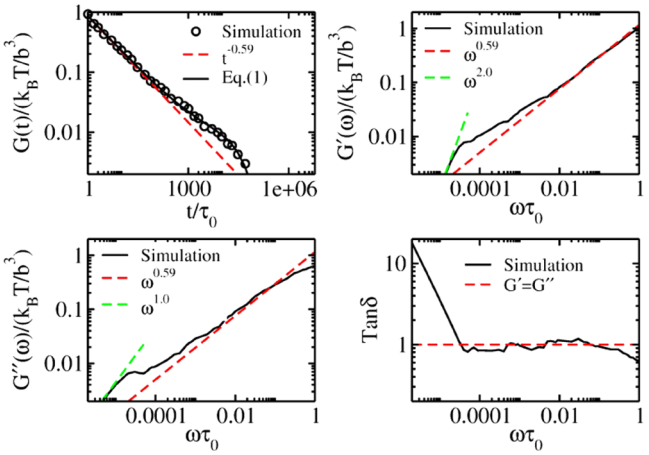


**Figure 1.** Stress relaxation modulus, $G_{HPM}(t)$, storage modulus, $G'_{HPM}(\omega)$, loss modulus, $G''_{HPM}(\omega)$, and loss tangent, $\tan\delta(\omega) = \frac{G''_{HPM}(\omega)}{G'_{HPM}(\omega)}$, of the baseline HPM.

baseline entangled polymer melt exhibits a tendency toward a plateau but not the full plateau that arises when polymer chains are in the highly entangled regime. In these simulations, the chosen chain length of polymers $L_C = 128$ is larger but not significantly than the estimated entanglement length of $L_e = 60-100$ for melts of bead-spring model chains using a FENE bond potential.[59] The following formula, including a smooth cross-over between the Rouse and reptation relaxation regimes, is adopted for fitting the direct simulation data of the stress relaxation modulus of the baseline HPM

$$G_{HPM}(t) = \left[C_m \times K_BT \times \left(\frac{t}{\tau_m}\right)^{\gamma} + G_e\right] \times \exp\left(-\frac{t}{\tau_{ter}}\right) \quad (5)$$

in which the fitting parameters are estimated ...numerically, with $\gamma \approx -0.59$, $G_e \approx 10^{-2}K_BT/b^3$, $\tau_m = 1.2\tau_0$, $\tau_{ter} = 2.5 \times 10^4\tau_0$, and $C_m = 0.83/b^3$, with $b$ and $\tau_0$ defined as the length and time units in the MD simulations, respectively. Therefore, we find that the corresponding entanglement length for our simulated HPM is approximately $L_e = C_m \times \frac{K_BT}{G_e} \approx 83$. The decay power $\gamma \approx -0.59$ indicates that, in our numerical HPM, the relaxation dynamics of polymer segments on contour lengthscales shorter than $L_e$, correspondingly at relaxation timescales $t \ll \tau_e$, deviates from the ideal Rouse relaxation with $\gamma = -0.5$.

The complex modulus, $G^*_{HPM}(\omega)$, is the Fourier transform of $G_{HPM}(t)$, with the storage (elastic) modulus $G'_{HPM}(\omega)$ and loss (viscous) modulus $G''_{HPM}(\omega)$ given by the real and imaginary parts: $G^*(\omega) = G'(\omega) + iG''(\omega)$, where $\omega = 2\pi/t$ is the angular frequency. Figure 1 gives the results for $G'_{HPM}(\omega) = \omega\int_0^\infty G_{HPM}(t) \times \sin(\omega t)dt$, $G''_{HPM}(\omega) = \omega\int_0^\infty G_{HPM}(t) \times \cos(\omega t)dt$, and the loss tangent, $\tan\delta(\omega) = \frac{G''_{HPM}(\omega)}{G'_{HPM}(\omega)}$, of the baseline HPM network. For any viscoelastic material, and for this baseline HPM in particular, the polymer melt is gel-like if $\tan\delta(\omega) < 1$ and sol-like if $\tan\delta(\omega) > 1$. As shown in Figure 1, there exists a low-frequency range where $\tan\delta(\omega) > 1$, indicating a sol-like behavior, a weak gel-like high-frequency behavior induced by polymer entanglements where $\tan\delta(\omega)$ is

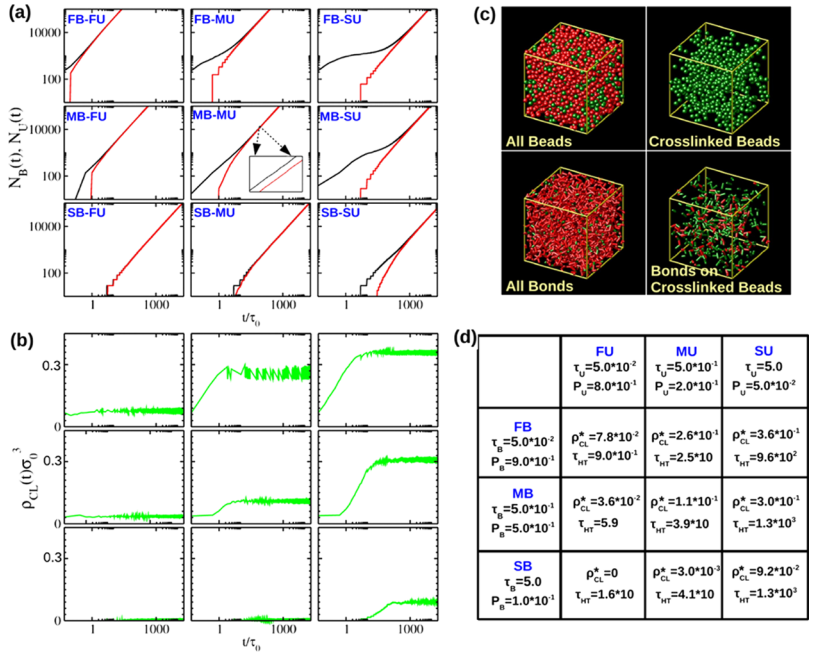


| | FU | MU | SU |
|---|---|---|---|
| | $\tau_U$=5.0*10$^{-2}$ $P_U$=8.0*10$^{-1}$ | $\tau_U$=5.0*10$^{-1}$ $P_U$=2.0*10$^{-1}$ | $\tau_U$=5.0 $P_U$=5.0*10$^{-2}$ |
| FB $\tau_B$=5.0*10$^{-2}$ $P_B$=9.0*10$^{-1}$ | $\rho^*_{CL}$=7.8*10$^{-2}$ $\tau_{HT}$=9.0*10$^{-1}$ | $\rho^*_{CL}$=2.6*10$^{-1}$ $\tau_{HT}$=2.5*10 | $\rho^*_{CL}$=3.6*10$^{-1}$ $\tau_{HT}$=9.6*10$^{2}$ |
| MB $\tau_B$=5.0*10$^{-1}$ $P_B$=5.0*10$^{-1}$ | $\rho^*_{CL}$=3.6*10$^{-2}$ $\tau_{HT}$=5.9 | $\rho^*_{CL}$=1.1*10$^{-1}$ $\tau_{HT}$=3.9*10 | $\rho^*_{CL}$=3.0*10$^{-1}$ $\tau_{HT}$=1.3*10$^{3}$ |
| SB $\tau_B$=5.0 $P_B$=1.0*10$^{-1}$ | $\rho^*_{CL}$=0 $\tau_{HT}$=1.6*10 | $\rho^*_{CL}$=3.0*10$^{-3}$ $\tau_{HT}$=4.1*10 | $\rho^*_{CL}$=9.2*10$^{-2}$ $\tau_{HT}$=1.3*10$^{3}$ |

**Figure 2.** Dynamics of bonds versus binding−unbinding affinities. In these simulations, transient binding and unbinding start from an equilibrium HPM absent of CLs. (a) $N_B(t)$ and $N_U(t)$ are running counts of the total number of CLs formed and broken up to time $t$, respectively. (b) $\rho_{CL}(t) = (N_B(t) - N_U(t))/V$ is the number density of transient bonds at time $t$, where $V$ is the system volume. (c) Snapshots (upper panels showing beads and lower panels showing bonds) of the quasi-stationary equilibrium structure for MB and unbinding kinetics. Here, noncross-linked (red) and cross-linked (green) beads are shown as spheres and covalent nearest-neighbor (red) and transient (green) bonds are shown as rods. (d) A table showing the quasi-equilibrium, time-averaged CL density, $\rho^*_{CL} = \langle\rho_{CL}(t)\rangle$ for $t > \tau_H$.



DOI: 10.1021/acs.jpcb.8b09357
J. Phys. Chem. B 2019, 123, 974−982

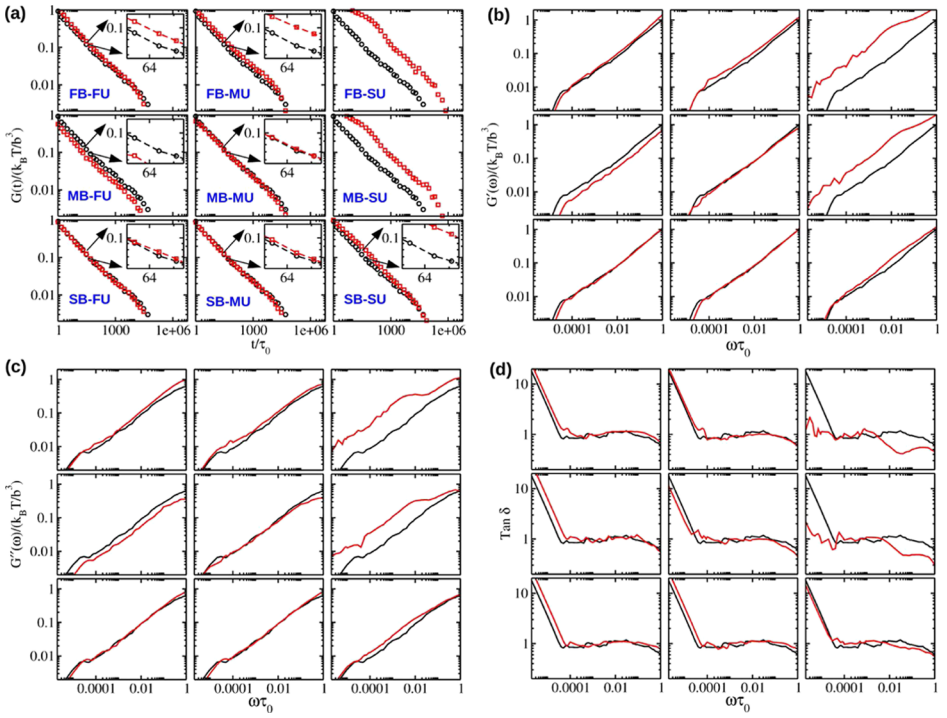


**Figure 3.** Transiently cross-linked polymer networks vs binding−unbinding affinities. (a) Stress relaxation modulus $G_{CL}(t)$; (b) storage modulus $G'_{CL}(\omega)$; (c) loss modulus $G''_{CL}(\omega)$; and (d) loss tangent $\tan\delta(\omega) = \frac{G''_{CL}(\omega)}{G'_{CL}(\omega)}$. All cross-linked features are shown in red, superimposed with the baseline HPM system features from Figure 1 in black.

slightly below 1, and then a broad intermediate-frequency range where $\tan\delta(\omega) \approx 1$, coincident with the power law scaling of $G_{HPM}(t)$. Next, we explore how these rheological properties are modified by transient CLs.

**Equilibrium Self-Healing Time and Average CL Density Versus Transient Binding−Unbinding Affinities.** The CLs are transient divalent bonds between pairs of non-nearest-neighbor beads on a chain. While every polymer bead is capable of participating in a transient bond, the imposed binding and unbinding kinetics will dictate two outcomes: (1) the equilibrium, or zero strain, self-healing time, $\tau_H$, defined as the time it takes starting from zero CLs to equilibrate to a mean number density of CLs; and (2) the time-averaged mean CL density, $\rho^*_{CL}$, and the amplitude of fluctuations about the mean. (In future studies, we will specify subsets of polymer chains available for transient binding by specific cross-linker species.) We coarsely divide the bond formation kinetics into three bins: fast binding (FB) (shortest $\tau_B$, highest $P_B$), medium binding (MB) (longer $\tau_B$, lower $P_B$), and slow binding (SB) (longest $\tau_B$, lowest $P_B$). Once again we coarsely divide the unbinding kinetics into three bins: fast unbinding (FU) (shortest $\tau_U$, highest $P_U$), medium unbinding (longer $\tau_U$, lower $P_U$), and slow unbinding (SU) (longest $\tau_U$, lowest $P_U$), defined analogously to the bond formation kinetics with specific values of $\tau_U$ and $P_U$ given in Figure 2d. These bins are equivalently described as short-lifetime, medium-lifetime, and long-lifetime bond duration regimes. At this coarse level of binding−unbinding affinities, a matrix of nine cases is explored: ($x$B, $y$U), where $x$ and $y$ are fast (F), medium (M), or slow (S). Figure 2d gives the matrix of outcomes, $\tau_H$ and $\rho^*_{CL}$, for all nine cases.

One discriminating characteristic of transient versus permanent cross-linked polymer networks is that the transient CL structure and mechanical strength are reversible, and thereby recoverable.[28−32] These materials self-heal by a combination of the relaxation and recovery modes (monomers, chains, and entanglements) of the baseline HPM and return to the quasi-stationary equilibrium of the CLs, after which we assumed that some event has broken all CLs.[28,29,37] (More generally, one could impose a criterion for CLs to break, e.g., a stress or strain threshold.[46]) All simulations begin at $t = 0$ from an equilibrated pure HPM with zero CLs. For each of the nine cases, we monitor the cumulative number of bonds that have formed, $N_B(t)$, and the cumulative number of bonds that have broken, $N_U(t)$; these counts are plotted in Figure 1a. The bond creation and destruction rates per unit time are $dN_B(t)/dt$ and $dN_U(t)/dt$, respectively. Note that, $\frac{dN_B(t)}{dt} > \frac{dN_U(t)}{dt}$ for early times $t > 0$ and the difference approaches 0 as $t$ grows. The first time, $\tau_H$, that the bond creation and destruction rates are equal defines the self-healing time of the network in the equilibrium state (with zero imposed strain). The number of CLs at any time $t$ is $N_{CL}(t) = N_B(t) - N_U(t)$. In Figure 2b, we show the time-dependent density of transient CLs, $\rho_{CL}(t) = N_{CL}(t)/V$. $N_{CL}(t)$ increases from $t = 0$ and then approaches and fluctuates about the plateau $N^*_{CL}$, the equilibrium mean number of CLs, for $t$ greater than $\tau_H$. Figure 2c shows simulation snapshots of the equilibrium structure of one transiently cross-linked system with intermediate or MB and unbinding kinetics. The self-healing time, $\tau_H$, and the mean equilibrium number density of CLs, $\rho^*_{CL} = \frac{N^*_{CL}}{V}$, are given in Figure 2d for all nine cases.

Two features emerge from Figure 2, which will serve to dictate the rheological consequences to follow: (1) $\tau_H$, the self-healing time, is sensitive to unbinding kinetics and relatively insensitive to unbinding kinetics. The shortest self-healing time arises when CLs form fast and break fast; this scenario



DOI: 10.1021/acs.jpcb.8b09357
J. Phys. Chem. B 2019, 123, 974−982

corresponds to a high concentration of weak, short-lived anchors between beads. The longest self-healing times arise when bonds are more permanent, that is, longer-lived. (2) $\rho^*_{CL}$, the CL density, is sensitive to both binding and unbinding kinetics, growing significantly as CLs last longer and form faster. The highest CL density arises when bonds form fast and persist, a scenario consisting of a high concentration of long-lived anchors.

**Dynamic Relaxation Modulus Versus Transient Binding−Unbinding Affinities.** In Figure 3, columns correspond to fixed CL lifetimes, showing the transition in $G_{HPM}(t)$ as bond formation goes from fast to slow, a proxy for cross-linker density going from high to low. Column 1, for short-lifetime bonds, reveals nonmonotonicity in the relaxation modulus versus CL formation affinity. There is a shift upward from the baseline for FB, with $G_{CL}(t) > G_{HPM}(t)$ for all $t$; there is a shift downward from the baseline for MB, with $G_{CL}(t) < G_{HPM}(t)$ for all $t$; finally, a shift back upward to recover the baseline for SB, showing a negligible effect on the baseline when bonds form slowly and are short-lived. These effects reflect the results from Figure 2, where the mean bond density is modest with fast bond formation, then drops in half with medium bond formation, and finally is negligible when bonds form slowly and have short lifetimes. The nonmonotonicity is an intriguing effect of short-lived bonds that we do not have a convincing explanation for, arising from the subtle interactions between the relaxation of chains and entanglements and the lengthscale distribution and persistence time between bead−bead transient CLs.

Column 2, for medium-lifetime bonds, reveals once again a nonmonotonicity in the relaxation modulus. From entry (1, 2), fast-forming bonds, there is a slightly bigger upward shift from the baseline than with short-lifetime bonds, entry (1, 1), reflecting the factor of 3 higher mean density of CLs from the same entries of Figure 2. Then, with medium bond formation, there is an apparently negligible effect on the relaxation modulus, even though the mean density of CLs is higher than any bond formation affinity with short lifetimes, column 1. With slow bond formation, there again is a negligible mean density of bonds, and likewise negligible effect on the relaxation modulus. These results are reinforced from the perspective of the rows, that is, the changes with respect to bond lifetimes rather than the affinity to form bonds, discussed below.

Column 3, for long-lifetime bonds, reveals the most dramatic effect, always shifting the transient network above the baseline. The greatest shift upward is for FB, which from Figure 2 column 3 has the highest mean density of CLs. The relaxation modulus slowly drops monotonically back toward the baseline as the propensity to bind weakens; nonetheless, the upward shift even at slow bond formation is greater than all short- or medium-lifetime bond settings in columns 1 and 2. These results from column 3 reveal an intuitive result that high-affinity, that is, long-time cross-linkers will have a very strong rheological impact on the baseline HPM, proportional to how fast CLs form, which is a proxy for the concentration of cross-linkers or the exposure of binding domains on the chains because of solvent quality, for example. The results in columns 1 and 2 are, in some sense, more intriguing, as they reveal the potential to shift rheology in different directions for short- and medium-lifetime cross-linkers by changing either the CL concentration or the chain conformations that either shield or expose binding domains to the population of binding molecules. Further details are revealed from the elastic and viscous moduli in frequency space, Figure 3b−d below.

The rows reveal trends for fixed propensity to form bonds as the lifetime of bonds goes from short to long; the study of these trends is a proxy for the effects due to increasing affinity of the cross-linker interactions with polymer domains. All three rows reveal a monotone increase in $G(t)$ for all $t$, that is, a shift upward in the relaxation modulus with increasing bond lifetimes. In row 1, fast-forming bonds (high concentrations of cross-linkers), all $G_{CL}(t)$ values are above the baseline, with the greatest overall shift upward among all nine cases, arising with fast-forming, long-lived bonds. In row 2, with medium bond formation timescales, $G_{CL}(t)$ is shifted down for short-lifetime bonds, shifts back up to approximately the baseline for medium-lifetime bonds, and shifts even higher for long-lifetime bonds with the second largest overall shift upward relative to the baseline.

*Elastic Modulus, That Is, Network Stiffness, Figure 3b.* We follow the relaxation modulus discussion with the columns first and then the rows. Column 1, for short-lifetime CLs, network strength is nonmonotonous with respect to bond formation affinity: $G'_{CL}(\omega)$ rises slightly above the HPM baseline for fast-forming CLs, then shifts below the baseline with medium bond formation affinity, then switches back to essentially recover the pure HPM strength when bond formation is slow. Column 2, for medium-lifetime bonds, network strength is again nonmonotonous with respect to bond formation affinity, but variations are less than with short-lifetime bonds. Column 3 reveals the most dramatic boosts in network strength arise with long-lived bonds, the biggest shift upward with fast-forming CLs, which drops a little with medium-forming CLs, and then drops close to baseline with slow-forming CLs.

Row 1, for fast-forming bonds, the network strength is always above the HPM baseline and increases monotonically with bond lifetime, first slightly above the HPM baseline strength for short-lifetime bonds, rising to higher strength for medium-lifetime bonds, then rising dramatically for long-lifetime bonds. This extreme result reflects a scenario in which bonds form quickly (e.g., due to a high concentration of cross-linkers) and last long, conditions that maximize CL density as shown in Figure 2, strengthening the network. Row 2, for medium affinity to form bonds (e.g., a medium cross-linker concentration), the network strength drops below the HPM baseline for short-lifetime bonds, a surprising result that we do not rigorously understand as noted earlier. Network strength increases monotonically with bond lifetime, first slowly with medium-lifetime bonds, and then dramatically with long-lifetime bonds, which is consistent with the relatively high CL density shown in Figure 2.

*Viscous Modulus, Figure 3c.* The viscous modulus $G''_{CL}(\omega)$ for all nine transient cross-linker cases follows the same trends, as well as the order of magnitude changes between slow, medium, and fast timescales to form and break bonds, as the elastic modulus, Figure 3b. The loss tangent, $\tan\delta = G''/G'$, reveals whether the network is more sol-like ($\tan\delta > 1$) versus gel-like ($\tan\delta < 1$) as a function of frequency. Although Figure 3b,c reveal trends in elastic and viscous moduli versus binding and unbinding affinities, the loss tangent captures the relative trends, as shown in Figure 3d. Recall the HPM baseline is sol-like for low frequencies, weakly gel-like for high frequencies, whereas $\tan\delta \approx 1$ over a wide medium frequency range. The most dramatic result arises with long-lived bonds, the first two entries of column 3: for fast and medium timescales of bond


DOI: 10.1021/acs.jpcb.8b09357
J. Phys. Chem. B 2019, 123, 974−982

formation, the low-frequency sol-like behavior is diminished, and a broad high-frequency gel behavior emerges, that is, the elastic moduli at all, but the mid-frequency range is amplified more than the viscous moduli. With long-lived and slow-forming bonds, col 3, entry 3, the low-frequency sol-like behavior returns, and the high-frequency HPM weak gel behavior is a little stronger. Columns 1 and 2 essentially reveal that the boosts or losses in $G''_{CL}(\omega)$ and $G'_{CL}(\omega)$ over these six entries are quantitatively similar, so tan $\delta$ remains close to the baseline HPM.

**Rescaling of the Transiently Cross-linked HPM Relaxation Modulus.** Whereas the network topology of permanently cross-linked polymers is stationary, the CL structure of a transient polymer network experiences relaxation. We define a relaxation time, $\tau_{rel}^{CL}$, relating to the lifetime of each transiently cross-linked network: (as revealed from tan $\delta$ in Figure 3d, converting now from frequency to time domain) the network is gel-like for $t < \tau_{rel}^{CL}$, beyond which the network transitions to an uncross-linked HPM-like behavior, with memory of the transient cross-linkers lost for $t > \tau_{rel}^{CL}$. The effective HPM-like relaxation dynamics starts at $t = \tau_{rel}^{CL}$, that is, $G_{CL}(t) = G_{HPM}^{eff}(t) = G_{HPM}(t/a_{shift})$ for $t > \tau_{rel}^{CL}$ with $a_{shift}$ being the horizontal shift factor of $G_{HPM}^{eff}(t)$ relative to $G_{HPM}(t)$. Note that, there is a corresponding relaxation time in the HPM, $\tau_{strand}^{HPM}$, which we refer to as the baseline relaxation time, for polymer strands with contour length equivalent to $S_{strand}^{CL}$, which is defined as the averaged contour length scale between CLs in transient networks. The averaged relaxation time of polymer strands changes from $\tau_{strand}^{HPM}$ in the HPM to $\tau_{rel}^{CL}$ in transiently cross-linked networks. Thus, we posit that there is an horizontal shift factor given by $a_{shift} = \frac{\tau_{rel}^{CL}}{\tau_{strand}^{HPM}}$. $G_{HPM}^{eff}(t)$ relative to $G_{HPM}(t)$ is compressed if $a_{shift} < 1$ or stretched if $a_{shift} > 1$. When $\tau_{rel}^{CL} > \tau_{strand}^{HPM}$, the dynamic relaxation modes corresponding to polymer segments with contour length scales longer than $S_{Con}^{CL}$ are prevented by the unrelaxed CL structure, that is, the structure "memory" of the polymer chains on these contour length scales are screened due to CLs. The corresponding relaxation modes do not start relaxing until the original CL structure of the transient polymer network is relaxed, for $t > \tau_{rel}^{CL}$. The relaxation of these modes is effectively stretched to longer timescales, by a shift factor $a_{shift} > 1$. On the contrary, when $\tau_{rel}^{CL} < \tau_{strand}^{HPM}$, the relaxation of the cross-linking structure induces an earlier relaxation of polymer strands between CLs occuring at $t = \tau_{rel}^{CL}$. In this case, the structure "memory" of polymer segments on the contour length scale of $S_{Con}^{CL}$ is lost by $t = \tau_{rel}^{CL}$, a timescale shorter than the baseline HPM relaxation time.

Note that the relaxation dynamics for entry (2, 1) (medium timescales to form bonds, short-lived bonds) experiences the longest delay in relaxation modulus, whereas entry (1, 3) (rapid bond formation, long-lived bonds) experiences the most accelerated relaxation modulus. As shown in Figure 4, the direct simulation data of $G_{CL}(t)$ for the cases of (MB, FU) and (FB, SU), can be rescaled to align with $G_{HPM}(t)$, where $a_{shift} > 1$ for the case of (FB, SU) and $a_{shift} < 1$ for the case of (MB, FU). This confirms our assumption that the relaxation dynamics of transiently cross-linked networks beyond the relaxation timescales of the cross-linking network structure is HPM-like with a horizontally shifted form of eq 1

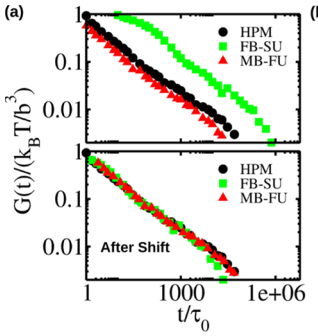


(b)

| | FU $\tau_U$=5.0*10$^{-2}$ $P_U$=8.0*10$^{-1}$ | MU $\tau_U$=5.0*10$^{-1}$ $P_U$=2.0*10$^{-1}$ | SU $\tau_U$=5.0 $P_U$=5.0*10$^{-2}$ |
|---|---|---|---|
| FB $\tau_B$=5.0*10$^{-2}$ $P_B$=9.0*10$^{-1}$ | $a_{shift}$=1.3 | $a_{shift}$=1.4 | $a_{shift}$=36 |
| MB $\tau_B$=5.0*10$^{-1}$ $P_B$=5.0*10$^{-1}$ | $a_{shift}$=0.45 | $a_{shift}$=1.0 | $a_{shift}$=14 |
| SB $\tau_B$=5.0 $P_B$=1.0*10$^{-1}$ | $a_{shift}$=1.0 | $a_{shift}$=1.1 | $a_{shift}$=2.6 |

**Figure 4.** (a) Stress relaxation modulus $G(t)$, for the baseline HPM in black, and transiently cross-linked HPMs, from entries of Figures 2 and 3: (1, 3) (FB times, long-lived bonds) in green and (2, 1) (MB times, short-lived bonds) in red. The upper and lower panel shows the simulated $G(t)$ from Figure 2 and the renormalization according to eq 2, respectively. (b) A table of the shift factor $a_{shift}$.

$$G_{CL}(t) = G_{HPM}(t/a_{shift}) = \left[C_m \times K_B T \times \left(\frac{t}{\tau_m \times a_{shift}}\right)^{\gamma} + G_e\right] \times \exp\left(-\frac{t}{\tau_{ter} \times a_{shift}}\right) \quad (6)$$

when $t > \tau_{rel}^{CL}$. At timescales of $t < \tau_{rel}^{CL}$, that is prior to the onset of HPM-like relaxation, the relaxation modulus of a transient network arises from combining the contributions of the relaxations of polymer segments (of length scale shorter than $S_{strand}^{CL}$) and the cross-linking structure of the transient network.[39,62] The unrelaxed CL structure of transient networks for $t < \tau_{rel}^{CL}$ is responsible for the plateau modulus of $G_{CL}(t)$ at short timescales that results in gel-like rheological characteristics at high frequencies as can be seen clearly for the cases of (FB, SU) and (MB, SU).

## DISCUSSION

Our goal is to explore the dynamics and quasi-equilibrium consequences by prescribing only the binding/unbinding probabilities of cross-linker proteins to all available active domains. We are exploring fewer assumptions for an important reason: in biology we do not know the underlying features (what subset of the polymers are active and with what available protein cross-linkers), so we are building a modeling framework that will allow us to learn the underlying features from sufficient experimental data. The imposed binding and unbinding kinetics dictate the time-averaged mean CL density and the time interval, from an initial broken cross-linked state, to converge to the stationary state (of mean and fluctuations of active CLs), that is central to self-healing and design of materials for regenerative medicine.[28−38] The mean density of active anchors, dictated by the transient binding affinities, gives direct insight into the rheological consequences relative to the baseline neat polymer melt. Both the recovery time and the density of CLs are proportional to the lifetime of the CLs (equivalently, the unbinding time). This is as expected because SU (slow unbinding) lowers the CL breaking rate $\nu_{break}(t)$ and raises the number of CLs $N_{CL}(t)$. Higher number of active CLs depletes inactive CLs which suppresses the CL creation rate $\nu_{create}(t)$. The convergence to equilibrium is thereby delayed with longer CL lifetimes. Therefore, the timescale for a CL to


DOI: 10.1021/acs.jpcb.8b09357
J. Phys. Chem. B 2019, 123, 974−982

unbind dominates the emergent transiently cross-linked network timescale $\tau_{equ}^{CL}$, which depends much less on the timescale to bind.

Aside from the details of the polymer chain model and chain length, and whether the network is unentangled, entangled, or highly entangled (which we do not explore), our model explicitly parametrizes the timescale affinities for binding and unbinding of active polymer domains by the cross-linker species. This framework reveals the binding−unbinding affinities that lead to prescribed conditions in the other models. We show, quantitatively, how the density of active CLs varies, according to binding and unbinding affinities. For example, a low density of CLs arises with SB (slow binding) and FU (fast unbinding) kinetics, and does not significantly alter the stress relaxation modulus $G(t)$ relative to the neat polymer melt. This result recovers the sticky reptation model prediction for a prescribed low concentration of transient CLs (closed stickers). For long-lived CLs, our simulations show that a plateau begins to emerge in $G(t)$ for timescales below the relaxation time of CLs. Correspondingly, a sol−gel transition emerges. This result is consistent with the sticky reptation result in which stickers act like permanent CLs on timescales below their relaxation time. Thus, $G(t)$ in our simulations has an emerging plateau with an elevation dictated by the density of CLs or the number of polymer strands between CLs. Colby and collaborators reached the same conclusion in their experimental work.[44,46] Our simulations further show that there is no structure change in $G(t)$ on timescales beyond the relaxation of CLs, except that the terminal relaxation time shifts longer, consistent with the theoretical and experimental results.[44,46−48]

Our simulations reveal a small yet measurable rheological difference on very small timescales between $G(t)$ for transiently cross-linked polymer networks and neat homopolymer melts. This was not discussed or predicted in theoretical papers,[44,46] yet was seen experimentally.[44,46] For short-lived bonds (FU kinetics), we reveal a nonmonotonicity in rheology with the binding timescale. This prediction has not, to our knowledge, been predicted or observed previously. As shown and mentioned above, the critical timescales related to the binding and unbinding kinetics of short-lived transient CLs is comparable with, or even smaller than the monomeric relaxation time $\tau_0$ of the neat polymer melt. We surmise that the effect of many short-lived CLs is to enhance the fluctuations of polymer chains, similar to an increase in system temperature. However, if the binding kinetics is too fast, previously bound bead pairs can rebind immediately after breaking, resulting in an effective increase in lifetime of the transient bonds. This result reveals the underlying kinetic basis of the nonmonotone rheology of transiently cross-linked polymer networks. The kinetics of short-lived bonds was addressed in the sticky reptation model work, yet the corresponding rheological consequences were not.

Note that the active cross-linker fluctuations are important as well, as that feature gives insight into the underlying fluctuations in the self-organization and structural morphology of the transiently cross-linked polymer network. This feature, while not expanded upon in the present study, has significant consequences for biology as it implies a source of enhanced thermal energy fluctuations that might very well affect the mobility of passive and active foreign particles or pathogens. We show that the morphology might be relatively stable and robust, or experience large fluctuations, as revealed in Figure 2b. Our future aim, as noted above, is to use modeling with as few assumptions as possible coupled with learning algorithms and experimental data to narrow down the uncertainty of the transient interactions in biological polymer networks.

## CONCLUSIONS

In this work, we have extended the open-source, computational MD platform LAMMPS to chart the rheological landscape spanned by transiently cross-linked, entangled polymer networks. The baseline network is a homogeneous melt of Rouse-like polymers above the entanglement concentration. Because of rate-limiting computational cost and time, we are not able to probe deep into the entanglement regime, although the presented chain length and concentrations are sufficient to capture important rheological consequences of transiently cross-linked, entangled polymer melts. Spanning fast, intermediate, and slow timescales of both binding and unbinding of the baseline network, we simulate convergence to quasi-equilibrium starting from an unstrained equilibrium with zero CLs. We postprocess the simulation data, tabulating the following statistical properties: the mean density of CLs and fluctuations about the mean, mean CL duration, and self-healing time (convergence time from initial configuration with zero CLs to quasi-equilibrium). With the quasi-equilibrium data, the Green−Kubo summation formula yields the dynamic relaxation modulus $G(t)$ for the HPM baseline over a $3 \times 3$ matrix of diverse of binding and unbinding kinetics (fast, medium, and slow for each). The Fourier transform of $G(t)$ provides the dynamic storage $G'(\omega)$ and loss $G''(\omega)$ moduli and loss tangent $\tan \delta = G''(\omega)/G'(\omega)$. These results reveal the rheological tuning induced by transient CLs on the CL-free baseline network. The two most salient results from these simulations are the following.

For sufficiently weak (short-lived) bonds, a remarkable nonmonotonicity emerges in the rheological features versus the affinity to form bonds. (The binding affinity is a proxy for cross-linker concentration or the accessibility of the cross-linkers to binding domains on the polymer chains.) We find that the relaxation modulus, viscous, and elastic moduli all shift above the baseline network if bonds form sufficiently fast; then all three features reverse and fall below the baseline as bonds form slower; and finally all features reverse direction again as bonds form very slowly, recovering back to the baseline rheology as bond formation timescales approach zero. This result implies rheological tuning capability in synthetic and biological polymer networks by controlling the concentration of cross-linkers or by controlling encounters of a fixed concentration of cross-linkers to attractive polymer domains.

For sufficiently strong (long-lived) bonds and sufficiently fast bond formation, a dramatic rise in the viscous and elastic moduli emerges at all frequencies, giving the strongest rheological modifications of the baseline network. Furthermore, the rises in dynamic moduli are marked by a greater amplification in the elastic moduli across the medium to high frequencies, inducing a sol−gel transition in this broad frequency range. These binding and unbinding conditions and consequences are intuitively understood when monitoring the equilibrium CL density, which is maximal when bonds form fast and break slowly. This particular result is reminiscent of airway mucus pathology, whereby healthy mucus undergoes a sol−gel transition during disease progression,[52] pointing to the potential role of additional or modified transient protein CLs in this transition.



DOI: 10.1021/acs.jpcb.8b09357
J. Phys. Chem. B 2019, 123, 974−982

From a theoretical polymer physics perspective, in the last section we sought to capture these rheological transitions through an effective rescaling of the baseline relaxation modulus across the 3 × 3 matrix of transiently cross-linked entangled polymer networks. The parameters in the scaling relation are based on the competition between the relaxation timescales of the baseline entangled polymer network and the CL-induced structure. By fitting the parameters in this rescaling formula, we show that all relaxation moduli with transient CLs approximately collapse onto the homogeneous polymer baseline modulus. From these results for a wide range of independent binding and unbinding affinities, one gains quantitative and qualitative intuition into how transient CLs tune a broad spectrum of rheological properties of entangled polymers. These results serve as yet another guide and complement to other coarse-grained modeling frameworks, with diverse applications including the design of synthetic polymer networks with transient molecular CLs, for example, vitrimers.[63−65] This study also serves as a guide to shift the rheology of biological entangled polymers by altering existing transient interactions or introducing new cross-linkers, for example, mucolytics.[17,19,20]

## AUTHOR INFORMATION


### Corresponding Author

*E-mail: forest@unc.edu.

### ORCID

Xue-Zheng Cao: 0000-0002-0409-6324


### Notes

The authors declare no competing financial interest.

## ACKNOWLEDGMENTS

This research was supported in part by the National Science Foundation through grants DMS-1462992, DMS-1517274, and DMS-1664645. The authors acknowledge valuable conversations with colleagues Kerry Bloom, Ronit Freeman, Boyce Griffith, David Hill, Jay Newby, and Sam Lai.

## REFERENCES


(1) Hult, C.; Adalsteinsson, D.; Vasquez, P. A.; Lawrimore, J.; Bennett, M.; York, A.; Cook, D.; Yeh, E.; Forest, M. G.; Bloom, K. Enrichment of Dynamic Chromosomal Crosslinks Drive Phase Separation of The Nucleolus. *Nucleic Acids Res.* **2017**, *45*, 11159−11173.

(2) Vasquez, P. A.; Hult, C.; Adalsteinsson, D.; Lawrimore, J.; Forest, M. G.; Bloom, K. Entropy Gives Rise to Topologically Associating Domains. *Nucleic Acids Res.* **2016**, *44*, 5540−5549.

(3) Albert, B.; Colleran, C.; Léger-Silvestre, I.; Berger, A. B.; Dez, C.; Normand, C.; Perez-Fernandez, J.; McStay, B.; Gadal, O. Structure-Function Analysis of Hmo 1 Unveils An Ancestral Organization of HMG-Box Factors Involved in Ribosomal DNA Transcription from Yeast to Human. *Nucleic Acids Res.* **2013**, *41*, 10135−10149.

(4) Prieto, J.-L.; McStay, B. Recruitment of Factors Linking Transcription and Processing of Pre-rRNA to NOR Chromatin is UBF-Dependent and Occurs Independent of Transcription in Human Cells. *Genes Dev* **2007**, *21*, 2041−2054.

(5) Wang, Y.-Y.; et al. Influenza-Binding Antibodies Immobilise Influenza Viruses in Fresh Human Airway Mucus. *Eur. Respir. J.* **2017**, *49*, 1601709.

(6) Theocharis, A. D.; Skandalis, S. S.; Gialeli, C.; Karamanos, N. K. Extracellular Matrix Structure. *Adv. Drug Deliv. Rev.* **2016**, *97*, 4−27.

(7) Wang, Y.-Y.; et al. IgG in Cervicovaginal Mucus Traps HSV and Prevents Vaginal Herpes Infections. *Mucosal Immunol.* **2014**, *7*, 1036−1044.

(8) Clarke, R. W.; Drews, A.; Browne, H.; Klenerman, D. A Single gD Glycoprotein Can Mediate Infection by Herpes Simplex Virus. *J. Am. Chem. Soc.* **2013**, *135*, 11175−11180.

(9) Lai, S. K.; Wang, Y.-Y.; Wirtz, D.; Hanes, J. Micro- and Macrorheology of Mucus. *Adv. Drug Deliv. Rev.* **2009**, *61*, 86−100.

(10) Desai, M. S.; et al. Dietary Fiber-Deprived Gut Microbiota Degrades The Colonic Mucus Barrier and Enhances Pathogen Susceptibility. *Cell* **2016**, *167*, 1339−1353.

(11) Birchenough, G. M. H.; Johansson, M. E. V.; Gustafsson, J. K.; Bergström, J. H.; Hansson, G. C. New Developments in Goblet Cell Mucus Secretion and Function. *Mucosal Immunol.* **2015**, *8*, 712−719.

(12) Hoegger, M. J.; et al. Impaired Mucus Detachment Disrupts Mucociliary Transport in A Piglet Model of Cystic Fibrosis. *Science* **2014**, *345*, 818−822.

(13) Ijssennagger, N.; Belzer, C.; Hooiveld, G. J.; Dekker, J.; van Mil, S. W. C.; Müller, M.; Kleerebezem, M.; van der Meer, R. Gut Microbiota Facilitates Dietary Heme-Induced Epithelial Hyperproliferation by Opening The Mucus Barrier in Colon. *Proc. Natl. Acad. Sci. U.S.A.* **2015**, *112*, 10038−10043.

(14) Maisel, K.; Ensign, L.; Reddy, M.; Cone, R.; Hanes, J. Effects of Surface Chemistry on Nanoparticle Interaction with Gastrointestinal Mucus and Distribution in The Gastrointestinal Tract Following Oral and Rectal Administration in The Mouse. *J. Controlled Release* **2015**, *197*, 48−57.

(15) Newby, J.; Schiller, J. L.; Wessler, T.; Edelstein, J.; Forest, M. G.; Lai, S. K. A Blueprint for Robust Cross-linking of Mobile Species in Biogels with Weakly Adhesive Molecular Anchors. *Nat. Commun.* **2017**, *8*, 833.

(16) Yuan, S.; et al. Oxidation Increases Mucin Polymer Cross-Links to Stiffen Airway Mucus Gels. *Sci. Transl. Med.* **2015**, *7*, 276ra27.

(17) Voynow, J. A.; Rubin, B. K. Mucins, Mucus, and Sputum. *Chest* **2009**, *135*, 505−512.

(18) Gross, A.; Torge, A.; Schaefer, U. F.; Schneider, M.; Lehr, C.-M.; Wagner, C. A Foam Model Highlights The Differences of The Macro- and Microrheology of Respiratory Horse Mucus. *J. Mech. Behav. Biomed. Mater.* **2017**, *71*, 216−222.

(19) Schenck, D. M.; Fiegel, J. Tensiometric and Phase Domain Behavior of Lung Surfactant on Mucus-like Viscoelastic Hydrogels. *ACS Appl. Mater. Interfaces* **2016**, *8*, 5917−5928.

(20) Thim, L.; Madsen, F.; Poulsen, S. S. Effect of Trefoil Factors on The Viscoelastic Properties of Mucus Gels. *Eur. J. Clin. Investig.* **2002**, *32*, 519−527.

(21) Sellers, L. A.; Allen, A.; Morris, E. R.; Ross-Murphy, S. B. Mechanical Characterization and Properties of Gastrointestinal Mucus Gel. *Biorheology* **1987**, *24*, 615−623.

(22) Norman, P. J.; et al. Sequences of 95 Human MHC Haplotypes Reveal Extreme Coding Variation in Genes Other than Highly Polymorphic HLA Class I and II. *Genome Res.* **2017**, *27*, 813−823.

(23) Ramaswamy, S. The Mechanics and Statistics of Active Matter. *Annu. Rev. Condens. Matter Phys.* **2010**, *1*, 323−345.

(24) Pollard, T. D.; Borisy, G. G. Cellular Motility Driven by Assembly and Disassembly of Actin Filaments. *Cell* **2003**, *112*, 453−465.

(25) Frantz, C.; Stewart, K. M.; Weaver, V. M. The Extracellular Matrix at A Glance. *J. Cell Sci.* **2010**, *123*, 4195−4200.

(26) Brangwynne, C. P.; Tompa, P.; Pappu, R. V. Polymer Physics of Intracellular Phase Transitions. *Nat. Phys.* **2015**, *11*, 899−904.

(27) Gasior, K.; Zhao, J.; McLaughlin, G.; Forest, G.; Gladfelter, A. S.; Newby, J. Partial Demixing of RNA-Protein Complexes Leads to Intradroplet Patterning in Phase-Separated Biological Condensates. *Phys. Rev. E* **2019**, *99*, 012411.

(28) Taylor, D. L.; in het Panhuis, M. Self-Healing Hydrogels. *Adv. Mater.* **2016**, *28*, 9060−9093.

(29) Phadke, A.; Zhang, C.; Arman, B.; Hsu, C.-C.; Mashelkar, R. A.; Lele, A. K.; Tauber, M. J.; Arya, G.; Varghese, S. Rapid Self-Healing Hydrogels. *Proc. Natl. Acad. Sci. U.S.A.* **2012**, *109*, 4383−4388.

(30) Tuncaboylu, D. C.; Sari, M.; Oppermann, W.; Okay, O. Tough and Self-Healing Hydrogels Formed via Hydrophobic Interactions. *Macromoleclues* **2011**, *44*, 4997−5005.




DOI: 10.1021/acs.jpcb.8b09357
J. Phys. Chem. B 2019, 123, 974−982

(31) Rosales, A. M.; Anseth, K. S. The Design of Reversible Hydrogels to Capture Extracellular Matrix Dynamics. *Nat. Rev. Mater.* **2016**, *1*, 15012.
(32) Haraguchi, K.; Uyama, K.; Tanimoto, H. Self-Healing in Nanocomposite Hydrogels. *Macromol. Rapid Commun.* **2011**, *32*, 1253−1258.
(33) Green, J. J.; Elisseeff, J. H. Mimicking Biological Functionality with Polymers for Biomedical Applications. *Nature* **2016**, *540*, 386−394.
(34) Mastorakos, P.; da Silva, A. L.; Chisholm, J.; Song, E.; Choi, W. K.; Boyle, M. P.; Morales, M. M.; Hanes, J.; Suk, J. S. Highly Compacted Biodegradable DNA Nanoparticles Capable of Overcoming The Mucus Barrier for Inhaled Lung Gene Therapy. *Proc. Natl. Acad. Sci. U.S.A.* **2015**, *112*, 8720−8725.
(35) Lorenz, J. S.; et al. Synthetic Transient Crosslinks Program The Mechanics of Soft, Biopolymer-Based Materials. *Adv. Mater.* **2018**, *30*, 1706092.
(36) Vatankhah-Varnosfaderani, M.; et al. Mimicking Biological Stress-Strain Behaviour with Synthetic Elastomers. *Nature* **2017**, *549*, 497−501.
(37) Stukalin, E. B.; Cai, L.-H.; Kumar, N. A.; Leibler, L.; Rubinstein, M. Self-Healing of Unentangled Polymer Networks with Reversible Bonds. *Macromolecules* **2013**, *46*, 7525−7541.
(38) Freeman, R.; Han, M.; Álvarez, Z.; Lewis, J. A.; Wester, J. R.; Stephanopoulos, N.; McClendon, M. T.; Lynsky, C.; Godbe, J. M.; Sangji, H.; Luijten, E.; Stupp, S. I. Reversible Self-Assembly of Superstructured Networks. *Science* **2018**, *362*, 808−813.
(39) Appel, E. A.; Tibbitt, M. W.; Webber, M. J.; Mattix, B. A.; Veiseh, O.; Langer, R. Self-Assembled Hydrogels Utilizing Polymer-Nanoparticle Interactions. *Nat. Commun.* **2015**, *6*, 6295.
(40) Tan, C. S. Y.; Agmon, G.; Liu, J.; Hoogland, D.; Janeček, E.-R.; Appel, E. A.; Scherman, O. A. Distinguishing Relaxation Dynamics in Transiently Cross-linked Polymeric Networks. *Polym. Chem.* **2017**, *8*, 5336−5343.
(41) Yesilyurt, V.; Ayoob, A. M.; Appel, E. A.; Borenstein, J. T.; Langer, R.; Anderson, D. G. Mixed Reversible Covalent Crosslink Kinetics Enable Precise, Hierarchical Mechanical Tuning of Hydrogel Networks. *Adv. Mater.* **2017**, *29*, 1605947.
(42) Tibbitt, M. W.; Appel, E. A.; Jayagopal, A.; Langer, R. Sustained Intravitreal Drug Delivery with Injectable Polymer-Nanoparticle Hydrogels. *Invest. Ophthalmol. Vis. Sci.* **2016**, *57*, 3651.
(43) Yesilyurt, V.; Webber, M. J.; Appel, E. A.; Godwin, C.; Langer, R.; Anderson, D. G. Injectable Self-Healing Glucose-Responsive Hydrogels with pH-Regulated Mechanical Properties. *Adv. Mater.* **2016**, *28*, 86−91.
(44) Chen, Q.; Huang, C.; Weiss, R. A.; Colby, R. H. Viscoelasticity of Reversible Gelation for Ionomers. *Macromolecules* **2015**, *48*, 1221−1230.
(45) He, Y.; Qiao, R.; Vatamanu, J.; Borodin, O.; Bedrov, D.; Huang, J.; Sumpter, B. G. Importance of Ion Packing on The Dynamics of Ionic Liquids during Micropore Charging. *J. Phys. Chem. Lett.* **2016**, *7*, 36−42.
(46) Zhang, Z.; Chen, Q.; Colby, R. H. Dynamics of Associative Polymers. *Soft Matter* **2018**, *14*, 2961.
(47) Leibler, L.; Rubinstein, M.; Colby, R. H. Dynamics of Reversible Networks. *Macromolecules* **1991**, *24*, 4701−4707.
(48) Rubinstein, M.; Semenov, A. N. Thermoreversible Gelation in Solutions of Associating Polymers. 2. Linear Dynamics. *Macromolecules* **1998**, *31*, 1386−1397.
(49) Baxandall, L. G. Dynamics of Reversibly Cross-Linked Chains. *Macromolecules* **1989**, *22*, 1982−1988.
(50) Watanabe, H.; Matsumiya, Y.; Kwon, Y. Dynamics of Rouse Chains Undergoing Head-to-Head Association and Dissociation: Difference between Dielectric and Viscoelastic Relaxation. *J. Rheol.* **2017**, *61*, 1151−1170.
(51) Watanabe, H.; Matsumiya, Y.; Masubuchi, Y.; Urakawa, O.; Inoue, T. Viscoelastic Relaxation of Rouse Chains undergoing Head-to-Head Association and Dissociation: Motional Coupling through Chemical Equilibrium. *Macromolecules* **2015**, *48*, 3014−3030.
(52) Hill, D. B.; et al. A Biophysical Basis for Mucus Solids Concentration (wt) as A Candidate Biomarker for Airways Disease: Relationships to Clearance in Health and Stasis in Disease. *PLoS One* **2014**, *9*, No. e87681.
(53) Chen, A.; McKinley, S. A.; Wang, S.; Shi, F.; Mucha, P. J.; Forest, M. G.; Lai, S. K. Transient Antibody-Mucin Interactions Produce a Dynamic Molecular Shield against Viral Invasion. *Biophys. J.* **2014**, *106*, 2028−2036.
(54) Marko, J. F.; Siggia, E. D. Polymer Models of Meiotic and Mitotic Chromosomes. *Mol. Biol. Cell* **1997**, *8*, 2217−2231.
(55) Kremer, K.; Grest, G. S. Dynamics of Entangled Linear Polymer Melts: A Molecular Dynamics Simulation. *J. Chem. Phys.* **1990**, *92*, 5057−5086.
(56) Plimpton, S. Fast Parallel Algorithms for Short-Range Molecular Dynamics. *J. Comput. Phys.* **1995**, *117*, 1.
(57) Dünweg, B.; Paul, W. Brownian Dynamics Simulations without Gaussian Random Numbers. *Int. J. Mod. Phys. C* **1991**, *02*, 817.
(58) Iwaoka, N.; Hagita, K.; Takano, H. Estimation of Relaxation Modulus of Polymer Melts by Molecular Dynamics Simulations: Application of Relaxation Mode Analysis. *J. Phys. Soc. Jpn.* **2015**, *84*, 044801.
(59) Lee, W. B.; Kremer, K. Entangled Polymer Melts: Relation between Plateau Modulus and Stress Autocorrelation Function. *Macromolecules* **2009**, *42*, 6270−6276.
(60) Likhtman, A. E.; Sukumaran, S. K.; Ramirez, J. Linear Viscoelasticity from Molecular Dynamics Simulation of Entangled Polymers. *Macromolecules* **2007**, *40*, 6748−6757.
(61) McLeish, T. C. B. Tube Theory of Entangled Polymer Dynamics. *Adv. Phys.* **2002**, *51*, 1379−1527.
(62) Meng, F.; Pritchard, R. H.; Terentjev, E. M. Stress Relaxation, Dynamics, and Plasticity of Transient Polymer Networks. *Macromolecules* **2016**, *49*, 2843−2852.
(63) Denissen, W.; Winne, J. M.; Du Prez, F. E. Vitrimers: Permanent Organic Networks with Glass-Like Fluidity. *Chem. Sci.* **2016**, *7*, 30−38.
(64) Pei, Z.; Yang, Y.; Chen, Q.; Wei, Y.; Ji, Y. Regional Shape Control of Strategically Assembled Multishape Memory Vitrimers. *Adv. Mater.* **2016**, *28*, 156−160.
(65) Fortman, D. J.; Brutman, J. P.; Cramer, C. J.; Hillmyer, M. A.; Dichtel, W. R. Mechanically Activated, Catalyst-Free Polyhydroxyurethane Vitrimers. *J. Am. Chem. Soc.* **2015**, *137*, 14019−14022.


DOI: 10.1021/acs.jpcb.8b09357
*J. Phys. Chem. B* 2019, 123, 974−982